Electrochimica Acta 513 (2025) 145608

Contents lists available at ScienceDirect

Electrochimica Acta

journal homepage: www.journals.elsevier.com/electrochimica-acta

Borohydride oxidation over Pt/C, Au/C and AuPt/C thin-film electrodes studied by rotating disk electrode and differential electrochemical mass spectrometry flow cell measurements

Zenonas Jusys [a,b,c], R. Jürgen Behm [a,d,*]

[a] Institute of Surface Chemistry and Catalysis, Ulm University, Albert-Einstein-Allee 47, D-89081, Ulm, Germany
[b] Helmholtz Institute Electrochemical Energy Storage Ulm (HIU), Helmholtzstr. 11, D-89081, Ulm, Germany
[c] Karlsruhe Institute of Technology (KIT), P.O. Box 3640, D-76021, Karlsruhe, Germany
[d] Institute of Theoretical Chemistry, Ulm University, Oberberghof 7, D-89081, Ulm, Germany

ARTICLE INFO

Keywords:
Borohydride oxidation
Transport effects
Mechanism
Kinetic isotope effects
RDE
DEMS
Pt/C catalyst
Au/C catalyst
AuPt/C catalyst

ABSTRACT

We report results of a systematic study of the borohydride oxidation reaction (BOR) in borohydride containing 0.5 M NaOH electrolyte over Pt/C, Au/C and AuPt/C thin-film catalyst electrodes, performed under enforced mass transport conditions. Employing rotating disk electrode (RDE) and thin-layer flow cell differential electrochemical mass spectrometry (DEMS) measurements, we identify kinetic limitations over a wide range of transport conditions. Together with the highly sensitive detection of evolved hydrogen as a function of potential, due to the use of a cold trap at the mass spectrometer inlet, this allows us to separate changes in the reaction selectivity, from complete to incomplete borohydride oxidation, from other kinetic limitations. Evaluation of the (apparent) number of electrons transferred per borohydride ion, both from the RDE measurements via the Koutecky-Levich formalism and from the DEMS measurements via the H_2 formation current, further supports the identification of complete borohydride oxidation (8 electron transfer) and incomplete oxidation (< 8 electrons transfer) reaction conditions. Using data on isotope labeled BD_4^- oxidation that we had published earlier, we identify weak secondary kinetic isotope effects for all catalysts, which indicate that B-H bond breaking does not represent the rate limiting step.

1. Introduction

Borohydride has attracted considerable attention as an alternative fuel for direct oxidation fuel cells due its low standard potential [1,2]. This would offer a higher theoretical voltage of the direct borohydride fuel cell (DBFC) or even twice higher for the borohydride-hydrogen peroxide DBFCs [3] compared to hydrogen-oxygen polymer electrolyte fuel cells (PEMFCs) [4]. DBFCs might also be a promising alternative for the direct methanol oxidation fuel cells (DMFC) [5]. Furthermore, the hydrogen-rich borohydride (four hydrogens per boron atom) can also be used as a source for a clean hydrogen production, which is generated by the bulk or catalytic hydrolysis of borohydride, as anode feed for a H_2/O_2 driven PEMFC [6,7]. This, however, may result in a reduced fuel utilization efficiency, since even under DBFC open-circuit conditions borohydride is consumed with unwanted H_2 release. Though the rate of borohydride bulk hydrolysis can be significantly slowed down at a high pH, in a strongly alkaline environment [8], which requires the employment of an anion exchange membrane in DBFCs, this cannot fully inhibit the catalytic hydrolysis [2]. Therefore, the complete oxidation of borohydride must be ensured by using a proper anode catalyst, which is active also for H_2 oxidation, to avoid the formation and escape of H_2 without further oxidation and the related efficiency losses [9]. Furthermore, it must be considered that the stepwise dehydrogenation and oxidation of borohydride toward the final product borate proceeds via a complex network of boron-hydrogen bond breaking and boron-oxygen bond making elementary steps [10]. This results in the formation of a number of reaction intermediates, which can be either oxidized further or escape without further oxidation, thus strongly affecting the fuel utilization [11,12]. These challenges have triggered a large number of theoretical [10,13–15] and experimental model studies [11,12,16–30], aiming at a better understanding of mechanistic and kinetic aspects of the electrooxidation of borohydride at different metals

* Corresponding author.
E-mail address: juergen.behm@uni-ulm.de (R.J. Behm).

https://doi.org/10.1016/j.electacta.2024.145608
Received 31 August 2024; Received in revised form 16 December 2024; Accepted 28 December 2024
Available online 28 December 2024

and alloys, which were summarized in recent reviews [9,31].

Previously, we reported results of a differential electrochemical mass spectrometry (DEMS) study, where employing isotope labeled borodeuteride we investigated the origin of the H_2 formed during borohydride oxidation – borohydride or water – as a function of the electrode potential and under open-circuit conditions in alkaline electrolyte [32]. Since platinum and gold are the common reference materials in both theoretical and experimental model studies of the borohydride oxidation reaction (BOR) and employed also in technical DBFC devices, carbon supported Pt and Au nanoparticle catalyst were used in that study. Furthermore, earlier studies had shown that bimetallic AuPt electrodes or catalysts, either prepared by co-deposition of Pt and Au by galvanic displacement of Ni [33] or using colloidal AuPt/C catalysts [34], can improve the catalytic activity of the elementary components in the BOR. This has stimulated already a number of further studies over AuPt (catalyst) electrodes, including Pt decorated gold nanoparticles [35] or Pt modified Au(111) electrodes [36]. In order to learn more about the performance of these bimetallic electrodes/catalysts under well-defined reaction and transport conditions, we included also carbon supported PtAu catalysts for comparison, using catalysts with metal particle sizes similar sizes to those of the other catalysts. For the same reason, the Au/C and AuPt/C catalysts were prepared via the same synthesis route, while a commercial Pt/C catalyst was used as reference. This earlier study revealed that hydrogen evolution (H_2, HD, D_2) is dominated by the reduction of H_2O (with trace amounts of HD) at potentials below 0.06 V (vs. RHE) over the Pt/C and AuPt/C catalysts, while there is no hydrogen evolution in the double-layer regime. Over the Au/C catalyst it only results from water reduction at $E < -0.2$ V (vs. RHE), while at higher potentials up to the oxide region only D_2 formation was observed. In the oxide region, over the metal oxide covered catalysts, there was only D_2 evolution from borodeuteride over the Pt/C and AuPt/C catalysts, while for Au/C also trace amounts of HD were detected. Additional measurements of the interaction between deuterated borohydride and the oxide pre-covered metal catalysts upon open-circuiting the electrode revealed a fast decay of the open circuit potential (OCP) to ca. -0.02 V (vs. RHE) for the Pt containing catalysts, with no gas evolution down to ca. 0.06 V, followed by a steep increase of H_2 evolution from water down to the steady-state OCP with a small amount of HD. Hence, under these conditions, water reduction is facilitated by electrons generated in the simultaneous borohydride oxidation, leading to the formation of a mixed potential. This electroneutral reaction is commonly referred to as a catalytic hydrolysis of borohydride. For the pre-oxidized Au/C electrode, the situation was more complex. D_2 is evolved during the potential transient via the reduction of a gold oxide by borodeuteride, as gold is not active for hydrogen oxidation. At the rest potential, there was no detectable H_2 evolution from water, due to the poor catalytic activity (= high overpotential) of gold for the hydrogen evolution reaction (HER) and for the BOR at a gold electrode. Thus, the mixed potential formed in this case results from very low rates of the HER and BOR, respectively, which fully agrees with an earlier report of a poor catalytic activity of a gold electrode in catalytic borohydride hydrolysis [37].

While that study provided detailed insights into a number of mechanistic aspects of the BOR at these catalysts, others, in particular, the role of mass transport and kinetic limitations, possible contributions from kinetic isotope effects or the impact of electronic modification on the performance of the bimetallic AuPt/C catalyst remained open. These are topic of the present study. Mass transport effects, which are of considerable interest since the borohydride oxidation rate is known to strongly depend on the mass transport [29], were studied in a rotating thin-film electrode (RDE) configuration [38] as a common hydrodynamic electrochemistry method. Potential dependent hydrogen formation, which provides information also on the selectivity of the BOR, as well as possible contributions from kinetic isotope effects to the Faradaic current, were investigated in a thin-layer flow cell in a DEMS setup, also under continuous electrolyte transport. In the following, after a brief description of the experimental details (Section 2), we will present and discuss the results of the RDE measurements (Section 3.1) and DEMS measurements (Section 3.2) performed on the same three carbon supported catalysts (Pt/C, Au/C and AuPt/C), which aim at resolving the above issues.

2. Experimental

As catalysts we used a commercial carbon supported Pt nanoparticle (Pt/C) fuel cell catalyst (20 % Pt/Vulcan XC72, E-TEK) and AuPt/C as well as Au/C catalysts prepared at the Center of Solar Energy and Hydrogen Research, Ulm (ZSW). In short, AuPt and Au nanoparticles were synthesized by thermal reduction of hexachloroplatinic and tetrachloroauric acid in oleylamine dispersion and loaded on the carbon black (Vulcan XC-72) support, following the procedure described by Lu et al. [39]. Careful catalyst characterization provided detailed information on the most important catalyst properties The mean particle sizes of the catalysts were 3.6 ± 1 nm (Pt/C) and 5.3 ± 0.8 nm (AuPt/C, Au/C), respectively [32]. For the AuPt/C catalyst, the Au:Pt ratio was 54:46. The metal loadings were 20 wt% (Pt/C), 25 wt% (AuPt/C), and 7.0 wt% (Au/C), respectively [32]. The lower metal loading of the Au/C catalyst was required due to the tendency of this catalyst to form larger particles at higher metal loadings.

Thin-film catalyst electrodes were prepared by pipetting and drying first a droplet of aqueous catalyst suspension (20 µl, 0.5 mg ml^{-1}, ultrasonically dispersed) onto a mirror-polished, removable glassy carbon disk (6 mm in diameter for the RDE head, 9 mm disks for DEMS, all from Sigradur G from Hochtemperatur Werkstoffe GmbH), followed by sequential pipetting and drying droplets of a highly diluted (1:50) aqueous Nafion (10 wt.%. Sigma Aldrich) solution. This sequential process with a much more diluted Nafion solution than used normally [38] resulted in an improved adherence of the catalyst film to the glassy carbon substrate and ensured a sufficient electrode stability in alkaline solution under enforced mass transport conditions, while maintaining a negligible diffusion resistance of the Nafion film. The resulting catalyst films were about 5 mm in diameter and, based on visual inspection, homogeneous.

The RDE measurements were conducted in a thermostated three-compartment electrochemical cell (23°C), using a Pine Instruments RRDE setup and five different rotation rates between 400 and 3600 rpm. A Pt wire counter electrode and a saturated calomel electrode (SCE) reference electrode, connected through a salt bridge, were used. All potentials are quoted vs. that of a reversible hydrogen electrode (RHE).

The simultaneous electrochemical and mass spectrometric DEMS measurements were performed in a dual thin-layer flow cell [40] equipped with a porous membrane (Scimat, 60 µm thick, 50 % porosity, 0.2 µm pore diameter) and an SCE reference electrode. Again, all potentials are quoted vs. that of the reversible hydrogen electrode (RHE). The working electrode potential was controlled and the currents were acquired by means of an AFRDE 5 (Pine Instruments) potentiostat/galvanostat, connected to a computerized data acquisition system. The concentrations of volatile species were simultaneously measured by a mass spectrometer (QMS 422, Pfeiffer Vacuum), after passing a liquid nitrogen cooled trap used to decrease the background signal of the m/z = 2 ion current resulting from the ionization of water vapor and subsequent recombination of the H species in the ion source of the mass spectrometer. The m/z = 2 ion current was calibrated in separate experiments for each catalyst in pure supporting electrolyte by stepping the electrode potential from the double-layer region to the hydrogen evolution region for one minute for and back to calculate the calibration constant $K^* = (2 \times I_{m/z=2}) / I_F$ [41].

The borohydride (Sigma Aldrich, ReagentPlus® 99 %) solutions in 0.5 M sodium hydroxide (Sigma Aldrich, semiconductor grade) were freshly prepared from sodium hydroxide and sodium borohydride (the latter was dissolved in 0.5 M solution of sodium hydroxide to prevent the bulk hydrolysis) in ultrapure water (Millipore Milli-Q, 18.2 MΩ cm). All solutions were deaerated by a flow of high purity (99.999 %) nitrogen

before and during the measurements.

3. Results and discussion

3.1. Rotating disk electrode (RDE) measurements

3.1.1. RDE measurements on a Pt/C catalyst electrode

The RDE measurements of the borohydride oxidation reaction (BOR) on the Pt/C thin-film electrode at different rotation rates are presented in Fig. 1 (solid lines), where the rotation rates are chosen such that based on the Levich equation [42] the increase in mass transport limited current should be constant between subsequent CVs traces. The BOR starts at rather low potential (*ca.* -0.015 V). It then increases steeply with increasing potential and approaches the mass transport limited current, reaching a maximum current at about 0.3 V. Note that the steep current increase points to very small or negligible Ohmic losses, which is in contrast to an earlier report [26]. With further increasing potential the current decreases slowly, followed by a steeper decay between 0.75 and 0.85 V, i.e., with the onset of PtO formation, where a distinct minimum is reached (Fig. 1a, solid lines). At even higher potentials, the current increases again, followed by a continuous decay up to the upper potential limit. All of these features are more pronounced at higher rotation rates.

In the negative-going scan (Fig. 1b, solid lines), the BOR current remains nearly constant in the PtO region until approaching the potential of PtO reduction, where the current again exhibits a distinct minimum. Note the by about 0.1 V lower potential of the current minimum compared to the positive-going scan. Subsequently, the current increases towards the mass transport limited value, which is essentially reached at potentials around 0.35 V. (The slightly lower current compared to the positive-going scan, which is independent of the rotation rate, is likely due to capacitive effects.) Then, the BOR current decreases slowly, followed by a steep decay at potentials lower than 0.05 V. At *ca.* -0.015 V, the current is no longer measurable. At this point, the BOR current is compensated by a similar size but opposite current resulting from the simultaneous hydrogen evolution reaction (HER) (see also Section 3.2).

Comparing these data with the BOR CVs reported for the same catalyst in Section 3.2 and in our earlier report [32], there seem to be significant differences. These can be simply explained, however, by the much lower electrolyte flow in the latter experiments, which leads to a significantly lower mass transport limited current, by about a factor of five to six, and thus to a much more pronounced representation of the adsorption / desorption features such as the H_{upd} and PtO reduction features (see also the CVs in Section 3.2). In a similar way, we can compare also with other data reported in the literature, which were recorded under different conditions on a smooth Pt electrode [25,30,43], and on Pt nanoparticles supported on either high surface area carbon [26] or carbon nanofilaments [12]. For the borohydride oxidation over a polycrystalline Pt electrode in the RDE setup, two distinct regions were reported, namely i) the potential region below Pt oxide formation, where the BOR occurs at close to the mass transport limit with about seven electrons transferred per borohydride and the formation/removal of BH_3OH^- results in kinetic limitations, and ii) the PtO potential region, where incomplete oxidation of borohydride occurs (5-6 electrons) with extensive evolution of hydrogen.

Based on RRDE measurements of the BOR on a Pt/C thin film electrode [12,26], where the authors investigated the role of the catalyst loading, rotation rate and other experimental parameters, they also proposed contributions from incomplete oxidation to BH_3OH^- at $E > 0.6$ V (RHE). This was concluded from the detection of oxidation currents at the Au ring electrode at 0.2 V, where Au is inactive towards BH_4^- oxidation, and from kinetic simulations [12], although formation of other oxidizable intermediates would be possible as well [18].

A more detailed discussion of the specific features in the BOR CVs will be given after comparison with measurements of the hydrogen oxidation reaction (HOR) over the Pt/C thin-film electrode in alkaline solution, which is purely mass transport limited over a wide potential range (Fig. 1, dashed lines). These HOR measurements are important for addressing the selectivity of the BOR, since complete (eight electron)

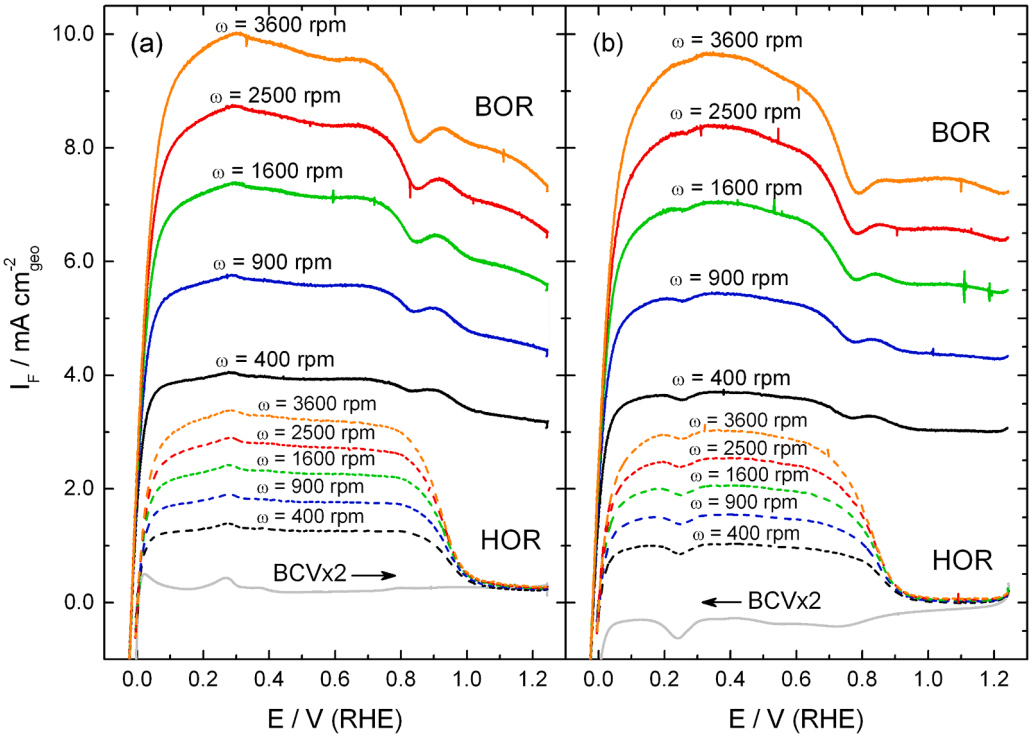

Fig. 1. RDE measurements of the BOR (full lines) and the HOR (dashed lines) over a Pt/C (E-Tek, 20 wt.%) thin-film electrode at different rotation rates (for rotation rates see figure) in the a) positive- and b) negative-going scans. Electrolyte: 1.0 mM $NaBH_4$ or H_2-saturated 0.5 M NaOH solution, potential scan rate: 10 mV s^{-1}, metal loading: 40 μg cm^{-2}, room temperature. Gray full lines: base cyclic voltammograms (10 mV s^{-1}) in a stagnant supporting electrolyte.

oxidation of borohydride is only possible for catalysts that are highly active for the HOR. This HOR measurement shows a well-defined mass transport limited current in the potential range from 0.05 to ca. 0.8 V in the positive-going scan (Fig. 1a, dashed lines) and from 0.05 to ca. 0.7 V in the negative-going scan (Fig. 1, dashed lines), with weak additional features due to hydrogen adsorption / desorption. These CVs are in good agreement with RDE data for the HOR over a polycrystalline Pt electrode in alkaline solution [44], which indicates also a minor impact of the Nafion film used for the preparation of the thin-film electrode on the diffusive H_2 transport. At potentials positive of 1.0 V (Fig. 1a, dashed lines), the HOR is largely suppressed on the Pt/C electrode, in contrast to the BOR, where the decay in this region is much less steep (Fig. 1, solid lines). This discrepancy agrees well with the previous finding of a change in the BOR selectivity in this potential range, over an oxidized Pt surface, which was derived from the onset of D_2 formation during the oxidation of borodeuteride [32]. This will be discussed in more detail in Section 3.2.

Furthermore, as would be expected for a purely mass transport controlled reaction, the mass transport limited HOR current increases with the square root of the rotation rate, resulting in constant spacings between the CVs at different rotation rates (Fig. 1 a, dashed lines). In contrast, in the BOR measurements this current increase with increasing rotation rate becomes gradually smaller (Fig. 1a, solid lines). While at 400 rpm, the BOR current is almost four times higher than the HOR current, as would be expected from the fourfold higher maximum number of electrons transferred in the BOR, this ratio is only about three at 3600 rpm. The relative decrease of the BOR current compared to the purely mass transport limited current points to increasing contributions from kinetic limitations. Such kind of kinetic limitations could arise, e. g., from the slower dehydrogenation of adsorbed borohydride or its incomplete dehydrogenation products, which would result in an increasing blocking of the electrode surface [12]. Alternatively, such effects could arise from a more effective removal of reactive reaction intermediates at higher rotation rates [12], due to a lower probability for re-adsorption and further reaction of desorbing intermediates [45]. Comparable effects had been reported also for borohydride oxidation on Pt/C catalyst layers of increasing thickness [21].

Based on these data and on previous findings on the BOR on Pt (catalyst) electrodes [12,25,26,29,30,43], the BOR CVs can be interpreted as follows: After the steep onset of the reaction at -0.015 V, the reaction rate continues to increase until reaching its maximum value. While for low transport conditions this maximum is essentially mass transport limited, higher mass transport results in increasing contributions from kinetic limitations. At higher rotation rates, these kinetic effects are active over the entire potential region, as evidenced by the decreasing separation when plotting the CVs versus the square root of the rotation rate. At low rotation rates, mass transport limitations seem to be reached at the current maximum at about 0.3 V. Hence, in both cases, kinetic limitations are present at low potentials, up to the current maximum at 0.3 V, and again at higher potentials. They increase continuously with increasing potential, up to 0.75 V, leading to a continuous decrease of the measured current. Based on our earlier DEMS report [32] and other reported data (see also Section 3.2), this current decrease is not due to a change to incomplete borohydride oxidation and H_2 formation, but must be due to kinetic limitation, as described above. At that point, the current decrease becomes steeper, which except for a bump at 0.9 V continues up to the upper potential limit of 1.25 V. This small bump is tentatively attributed to OH uptake / oxide formation on the Pt surface. Considering the observation of increasing hydrogen formation at >0.75 V [32], this decrease must at least partly be due to a change in BOR selectivity with increasing potential. But based on the constant hydrogen formation rate at > 1.0 V [26,32], also other kinetic effects must play a role in the potential range > 1.0 V. Nevertheless, the BOR can proceed at a rather high rate even on the PtO covered electrode, in contrast to the HOR, where the rates become very low at > 1.0 V (Fig. 1).

In the negative-going scan, the current is about constant up to the onset of PtO reduction, which is in contrast to the decay in the positive-going scan in this potential range. Reduction of the PtO cover layer, which is indicated by the current minimum at little below 0.8 V, leads to an increase in BOR activity and a concomitant change in BOR selectivity. This minimum contains contribution from PtO reduction and borohyride oxidation. Different from the positive-going scan, hydrogen formation continues up to about 0.65 V (see also Section 3.2). This reflects the well-known hysteresis in Pt oxidation / reduction. Further decrease of the potential results in a continuing slow increase of the current, until reaching the maximum value. Even in this potential range, after complete reduction of the catalyst on the one hand and before the onset of H adsorption on the other hand, the current traces in the positive-going and negative-going scan are not identical, indicative of ongoing differences in the surface composition in the two scan directions.

In summary, these RDE measurements clearly revealed that despite of the high activity of the Pt/C catalyst for the BOR in the potential range between 0.6 and 1.0 V, kinetic limitations become increasingly important also in this regime under high-transport conditions. At lower potentials, down to the onset of the reaction at about -0.015 V and at higher potentials, in the PtO region, the kinetic limitations are considerable also at lower transport conditions.

3.1.2. RDE measurements on a Au/C catalyst electrode

Similar measurements performed with a Au/C thin-film electrode at different rotation rates (Fig. 2, solid lines) show barely any BOR activity up to *ca.* 0.2 V, in agreement with previous reports on borohydride oxidation at a gold electrode [10,16,18,20,24,26,37,43]. At potentials positive of 0.2 V, the oxidation current increases exponentially. This is different from the Pt/C catalyst, where the initial current increase is much steeper. The maximum current, which is reached in the potential region between 0.9 and 1.1 V, is about one third lower than that for the Pt/C electrode (Fig. 1, solid lines), indicative of considerable kinetic limitations and/or contributions from incomplete borohydride oxidation even in this potential region. This fully agrees with our previous detection of hydrogen formation from borohydride over the entire potential range where the BOR is active [32]. At more positive potentials, the current decreases significantly, which we relate to the onset of Au oxide formation (see Fig. S4) and the resulting lower BOR activity / change in BOR selectivity by the oxidic surface layer developed at higher potentials. Nevertheless, also in this case the BOR is active on the oxide covered catalyst. Changes in the BOR selectivity under these conditions, while oxidizing BH_4^- on a polycrystalline Au disc electrode, were detected in previous RRDE shielding measurements from the oxidation of the reaction intermediates $BH_3(OH)^-$, $BH_2(OH)_2^-$ or other intermediates at the Au ring electrode [18,26]. Oxidation of borohydride and of other active species present, such as BH_3OH^- formed by hydrolysis, on the hydroxide / oxide covered Au surface was postulated also based on electrochemical quartz crystal microbalance measurements [24].

In the negative-going scan, the oxidation current first decreases, passes through a minimum and only then increases, which seems to be in contrast to the continuous decay in the positive-going scan. This discrepancy can be easily understood when considering that also during the negative-going scan Au surface oxidation initially continues, as indicated by a positive current in the base CV (see also Fig. S4), which results in a further decrease in the BOR current. Reduction of the Au surface oxide, which in the BCV is indicated by a change to negative currents, sets in only at the current minimum at about 1.3 V. This leads to the expected continuous current increase up to the range of the current maximum, in the plateau at 0.9 – 1.1 V. For further decreasing potential the current passes through a clearly resolved shoulder at about 0.6 V, before disappearing at about 0.2 V. This shoulder was not resolved in the positive-going scan in the present measurements, but is visible also there when going to slower transport conditions (Section 3.2 and ref. [26,32,46,47]). Based on earlier reports [17,47], the resolution of

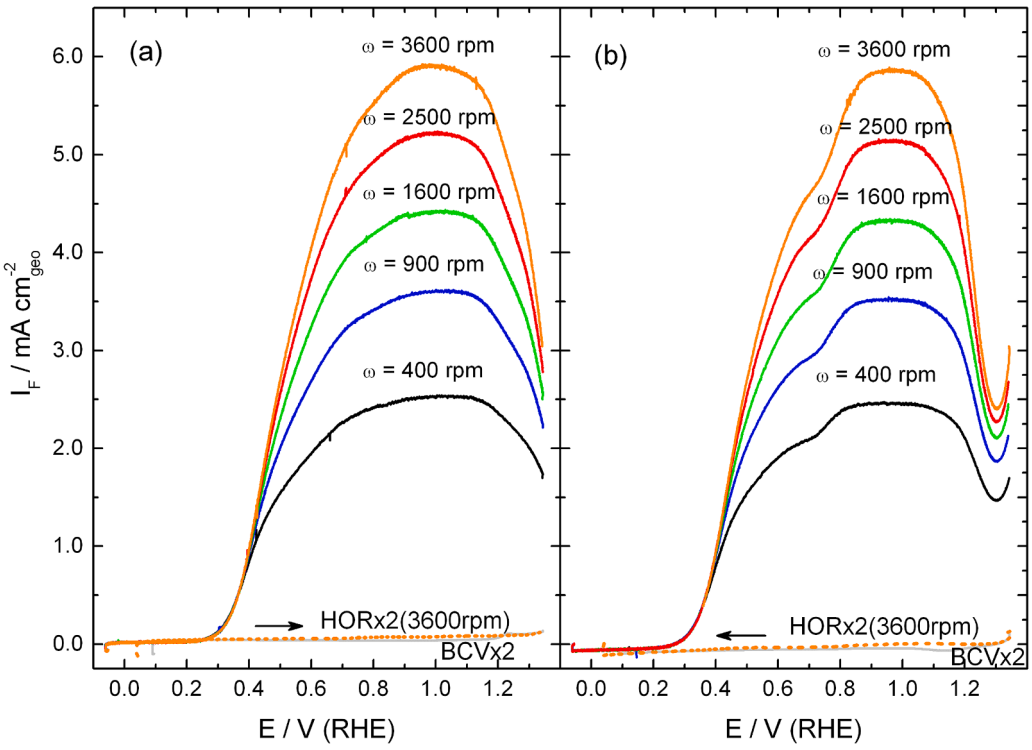

Fig. 2. RDE measurements of the BOR and the HOR (dashed lines) over a Au/C (ZSW, 8 wt.%) thin-film electrode at different rotation rates (for rotation rates see figure) in the a) positive- and b) negative-going scans. Electrolyte: 1.0 mM $NaBH_4$ in 0.5 M NaOH, potential scan rate: 10 mV s^{-1}, metal loading: 15 μg/cm^{-2}, room temperature. Gray lines: base cyclic voltammograms (10 mV s^{-1}) in a stagnant supporting electrolyte.

this shoulder depends also on the concentration of BH_4^-, with a better resolution obtained at lower concentrations. Furthermore, our DEMS measurements revealed also a higher hydrogen formation rate, relative to the measured Faradaic current, in this peak than at higher potentials, indicating a change in BOR selectivity between this shoulder and the peak maximum, both in the positive-going and negative-going scan. Similar to the trend in the Faradaic current, this effect is more pronounced in the negative-going scan (Section 3.2). This DEMS result fits well also to an earlier proposal by Chatenet et al. [47], who based on RDE and impedance spectroscopy (EIS) measurements derived that these features, the main plateau at 1.1 - 0.9 V and the shoulder at about 0.6 V, reflect a change in BOR selectivity.

The increase in the maximum current for the BOR over the Au/C catalyst with increasing rotation rate follows that observed in the positive-going scan (Fig. 2b). Thus, the maximum current is more than one third lower than the mass transport limited current at the highest rotation rate. Furthermore, in both scan directions the BOR current does not follow the trend expected from the Levich equation, which would result in constant current increases between the maximum currents of the CVs for the different applied rotation rates. As discussed already for Pt/C, this can be explained by rotation rate dependent contributions from incomplete borohydride oxidation, due to increasing off-transport of partial oxidation products with increasing rotation rate [45]. The conclusion of incomplete oxidation in the BOR over Au/C is supported also by the well-known low activity of gold in the HOR [48], which inhibits the oxidation of hydrogen released during the reaction (see also Section 3.2). The close correlation between the HOR activity and the ability for complete oxidation of borohydride is supported also by the RDE measurements over a Ag/C catalyst, which showed a comparable activity for the BOR as Au/C and no activity for the HOR [19].

In summary, these RDE measurements clearly revealed significant kinetic limitations in the BOR on a Au/C catalyst over the entire potential range the BOR is active, including the range of AuO formation at high potentials. They are more pronounced at higher rotation rates, but occur also under low-transport conditions. Also, their effects are more pronounced at lower potentials, between the high current range (0.8 – 1.0 V) and the onset of the reaction at about 0.2 V, and at higher potentials, in the Au oxide region.

3.1.3. RDE measurements on a AuPt/C catalyst electrode

In a last set of RDE measurements, we characterized transport effects in the BOR on a AuPt/C thin-film electrode at different rotation rates (Fig. 3, solid lines). Similar to the BOR on Pt/C, the reaction starts at low potentials (*ca.* -0.015 V) and increases steeply with the potential up to *ca.* 0.1 V. The further current increase with increasing potential in the potential region of H_{upd} on Pt, however, is not as steep as that on Pt. The currents achieved in the low potential region from 0.0 to 0.4 V (Fig. 3, solid lines) are about half of those obtained on the Pt/C electrode (Fig. 1, solid lines). Also the maximum current, which depending on the rotation rate is reached between 0.8 and 0.9 V, is significantly less, by more than one third, than the currents derived from the measurements on Pt/C, indicative of considerable kinetic limitations also for reaction on this catalyst. In fact, they are comparable to those obtained for the Au/C catalyst (Fig. 2). In the low-potential region, however, the BOR activity of the AuPt/C catalyst is much higher than that of the Au/C catalyst (Fig. 2), which is inactive up to *ca.* 0.2 V, indicating that the activity of the AuPt/C catalyst under these conditions is largely driven by the Pt surface atoms / ensembles (Pt sites). With further increasing potential, the current traces largely follow those obtained for the Au/C catalyst electrode.

In the negative-going scan (Fig. 3b), we find the characteristic current minimum mentioned already for the BOR on the Au/C catalyst electrode, and also the subsequent current increase down to about 1.0 V related to the reduction of the Au oxide. Hence, the characteristics in this part of the CVs seem to be dominated by the reaction behavior of Au-O sites. With further decreasing potential, however, the current increases again significantly, reaching a maximum at about 0.6 V. This increase is particularly pronounced for high rotation rates. This transport

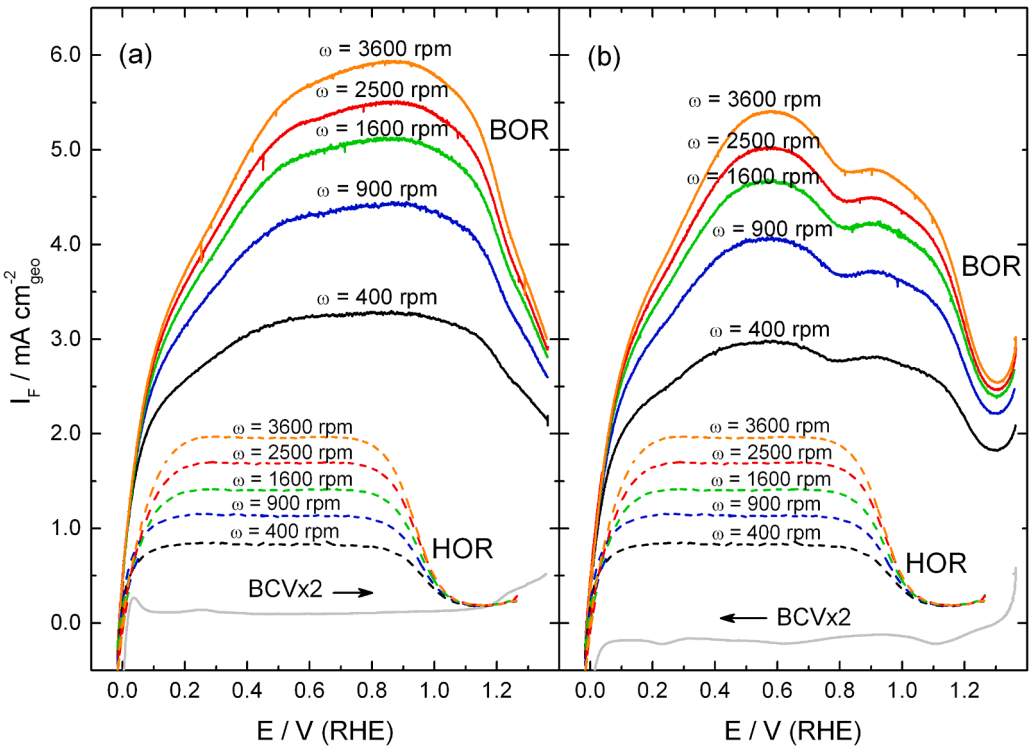

Fig. 3. RDE measurements of the BOR (full lines) and HOR (dashed lines) over a AuPt/C (ZSW, 25 wt.%) thin-film electrode at different rotation rates (for rotation rates see figure) in the a) positive- and b) negative-going scans. Electrolyte: 1.0 mM $NaBH_4$ or H_2-saturated 0.5 M NaOH, potential scan rate: 10 mV s^{-1}, metal loading: 50 μg cm^{-2}, room temperature. Gray full lines: base cyclic voltammograms (10 mV s^{-1}) in a stagnant supporting electrolyte.

dependence seems to be the reason also why this pronounced lower potential feature was not resolved in the DEMS measurements in Section 3.2 and in ref. [32], which were performed at much slower transport conditions (see also Section 3.2). Since there are shoulders at about this potential both for the Au/C and the Pt/C catalysts in the negative-going scan, it is not directly obvious whether this peak is related to Au sites or to Pt sites. Considering, however, that for the BOR on Au/C the current at 0.6 V is much lower than at the current maximum, we tend to associate this feature with the BOR on Pt dominated sites.

Significant modifications in the BOR activity of Pt or Pd upon alloying with gold or silver were reported also for AuPd/C [37] and AgPt/C [19] nanoparticle catalyst electrodes. On these bimetallic catalysts, the reaction behavior may be affected by a number of different effects, including geometric ensemble effects [49], electronic ligand [50, 51] and electronic strain effects [52]. For a recent review of such effects see ref. [53]. Ensemble effects may slow down the reaction rate by the limited abundance of larger Pt_n ensembles, if these are required for the reaction. This is particularly true at lower surface concentrations of the respective metal. Electronic modifications of the metals, by interaction with neighboring metal atoms or by strain, may affect the adsorption energies and kinetic barriers on the otherwise same site [54]. For pseudomorphic PtAu films on Pt(111), electronic ligand and strain effects were shown to essentially compensate each other for the adsorption of H, OH [55] and CO [56], while CO adsorption on a pseudomorphic PtAu layer on Au(111) with its larger lattice size is stabilized [57]. Considering also the relation between adsorption energy and activity in a catalytic reaction given by the Sabatier relation [58], it is not surprising that the BOR activity of the mixed AuPt/C catalyst is not just a down-scaled version of the Pt/C activity, but also shows a different potential dependence. This interpretation in terms of a modified activity of the Pt sites is in line with the nearly unchanged BOR activity at potentials from 0.8 to 1.0 V for the AuPt/C catalyst (Fig. 3, solid line), compared to the slow decay of the activity in this potential region for the Pt/C catalyst (Fig. 1, solid lines). At higher potentials, on the other hand, the loss of the BOR activity of the AuPt/C catalyst (Fig. 3, solid lines) seems to be mainly related to the deactivation of the gold sites due to gold oxide formation, with a rather steep decay at high potentials above 1.1 V, in contrast to the slow decay over Pt/C starting already at about 0.7 V (Figs. 1 and 2, solid lines). Also in the low-potential region, between the steep onset of the BOR up to 0.1 V and 0.6 V, the BOR behavior of the AuPt/C catalyst (Fig. 3a, solid lines) differs from that of the Pt/C catalyst (Fig. 1a, solid lines), indicative of synergistic effects arising from the presence of both metal species at the surface. In this case, the increase with potential is much slower than for the Pt/C catalyst. In total, the BOR on this catalyst seems to be dominated by reaction on electronically modified Pt sites at potentials between 0.1 and 1.0 V and on (oxide covered) Au sites at higher potentials. A more quantitative understanding of these aspects would require, however, detailed information on the surface concentrations of Au and Pt atoms and on their lateral distribution [53].

Synergistic features, related to the presence and interaction of both metals, appear also in the HOR over the AuPt/C catalyst (Fig. 3, dotted lines). In contrast to the Au/C catalyst electrode, which is essentially HOR inactive, the AuPt/C electrode displays a considerable HOR activity, although it is more than one third lower than that of the Pt/C catalyst (Fig. 1, dotted lines). Hence, there are considerable kinetic limitations also for this reaction. These are most likely due to a lack of active Pt sites per exposed geometric area for the former case. Here we note that we neither know the exact nature (ensemble size) of the active sites for the HOR (for a general discussion see refs. [55] and [59]) nor the surface composition of the AuPt/C catalysts. Therefore, we can only provide a rough estimate of the number of adsorption sites on this catalyst surface from the H underpotential deposition features in the base CV (Fig. S3, S5), which results in a relative H_{upd} uptake (per metal surface area) of about one fifth of that of the Pt/C electrode. Furthermore, the mass transport dominated flat region for the HOR extends to more positive potentials for the AuPt/C catalyst (Fig. 3, dashed lines) than that for the Pt/C catalyst (Fig. 1, dashed lines), while in the

low-potential region the HOR starts to decay already at potentials lower than 0.2 V for the AuPt/C catalyst (Pt/C: 0.15 V), which is likely due to a combination of fewer active Pt sites and modifications of the electronic properties of the alloyed metals.

In summary, the RDE measurements revealed synergistic effects in the BOR, caused by the interaction of Pt and Au surface atoms, as compared to a superposition of Pt- and Au-typical reaction characteristics. In the low-potential region, up to the flat maximum in the potential range 0.8 – 1.0 V, the BOR seems to be dominated by the reaction on electronically modified Pt sites, while in the oxide region it is more Au-like. The lower number of highly active Pt sites leads to an increased contribution of kinetic limitations compared to Pt/C, with a maximum current of about 60 % of that on Pt/C.

The HOR measurements allowed us to determine the mass transport limited current, which is identical for all catalysts. Considering the higher number of electrons, it should be four times higher for the BOR, assuming complete oxidation of borohydride. Since on the other hand the diffusion coefficient of BH_4^- anions is lower than that of H_2 (D_{BH4} = 16.7 - 35±3.5 × 10^{-6} cm^2 s^{-1} [43,60,61], D_{H2} = 40 - 45 × 10^{-6} cm^2 s^{-1} [62–64]), the difference should be slightly less. Furthermore, the measurements clearly demonstrated that the BOR can proceed also over the oxidized electrodes, where the HOR is inhibited, though at lower rates.

3.1.4. Electron transfer in the BOR on the different catalyst electrodes

The number of electrons transferred in the BOR per BH_4^- species consumed was calculated from Koutecky-Levich plots of at the respective potentials according to [37]. For this analysis, we used values 1.95 × 10^{-5} cm^2 s^{-1}, and 1.19 × 10^{-2} cm^2 s^{-1} [61]) for the diffusion constant D of BH_4^- and for the kinematic viscosity ν, respectively. The value of the diffusion constant D, which is in the range of the different values reported in the literature [43,60,61 and close to that determined by Denuault et al. (D = 1.67 × 10^{-5} cm^2 s^{-1}) [60], was arranged such that the theoretical limit of 8 electrons per BH_4^- (complete oxidation) was not exceeded on the different catalysts. The quality of the fits is illustrated in a representative Koutecky-Levich plot in Fig. S1 in the Supplementary Materials. The data in Fig. 4 represent averages of the positive- and negative-going scans, which differ by their contributions from double-layer charging to the measured current. Data obtained from the individual scans are presented in Fig. S2.

The number of electrons transferred in the BOR per BH_4^- species consumed on the Pt/C catalyst, is plotted in Fig. 4a. The value of approximately 7.2 electrons in the potential range from 0.05 to 0.8 V corresponds to almost complete oxidation of borohydride to borate with a release of eight electrons (complete oxidation of borohydride) according to the general Eq. (1).

$$BH_4^- + 8\ OH^- \rightarrow BO_2^- + 6\ H_2O + 8\ e^- \quad (1)$$

In the PtO region, at ≥ 0.8 V, this number decays to ca. 6.1, indicative of a change in the selectivity, which is in full agreement with the decay of the current in the RDE measurements in Fig. 1 and the observation of hydrogen formation in [32] (see also Section 3.2). Less than eight electrons transferred per BH_4^- ion indicate an incomplete oxidation over this catalyst according to the general Eq. (2):

$$BH_4^- + x\ OH^- \rightarrow BO_2^- + (x - 2)H_2O + (4 - x/2)H_2 + x\ e^- \quad (2)$$

Hence, despite of the complexity of the multistep reaction, the evaluation via the Koutecky-Levich results in similar trends as deduced from the Faradaic current and the hydrogen formation.

For the Au/C catalyst (Fig. 4b), we find a significantly lower electron transfer at the onset of the reaction at ca. 0.5 V of ca. 4.0 electrons per BH_4^-, which increases to about 4.9 electrons at ca. 0.8 V. This is followed by a plateau at this level up to ca. 1.1 V. This plateau corresponds to the flat region in the measured current between 0.9 and 1.1 V (in the negative-going scan). In the oxide region, at potentials above 1.15 V, the number of electrons transferred decreases to about 4.4. The generally

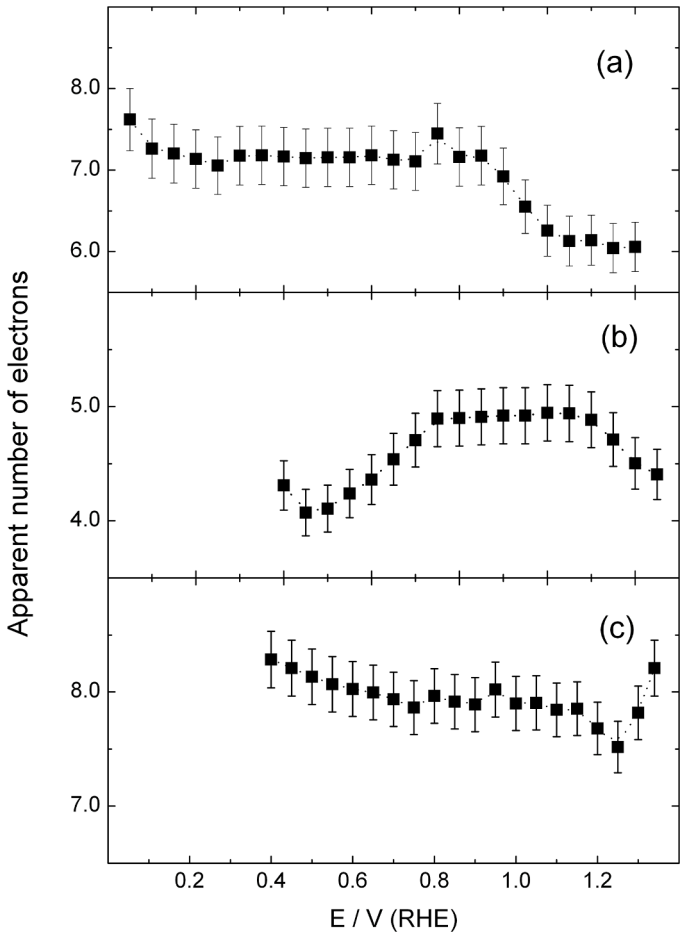

Fig. 4. Average number of the apparent number of electrons transferred per BH_4^- over: a) Pt/C (E-Tek 20 wt.%); b) Au/C (ZSW, 8 wt.%); c) AuPt/C (ZSW, 25 wt.%) thin-film electrodes during the positive-going and negative-going scans, calculated from the data of Figs. 1–3 using the Koutecky-Levich formalism. Experimental parameters are given in Figs. 1–3. Error bars indicate a ±4 % spread.

lower number of electron transferred goes along with the low activity of Au to oxidize hydrogen, leading to the release of H_2 in the BOR at the Au/C catalyst ([32] and Section 3.2), as expected from the Eq. (2). The release of H_2 can be rationalized by the negligible activity of Au electrodes for the adsorption and oxidation of hydrogen (see also Section 3.2) [48]. Here it is interesting to note that the difference in the maximum Faradaic current obtained on the Au/C and Pt/C electrodes is less than the 25 % given the lower electron number on Au/C, which points to additional kinetic barriers in the BOR on the latter electrode. Furthermore, the much smaller difference between the currents in the positive- and negative-going scan than obtained for the other two catalysts (see Fig. S2) indicates much smaller contributions from double-layer charging.

Finally, for the AuPt/C catalyst (Fig. 4c), the average number of electrons in the plateau region is about eight, with slightly higher values in the low-potential range below 0.4 V. At potentials above 1.15 V, the number of electrons decreases, indicative of increasing contributions from incomplete borohydride oxidation. Possible reasons for the apparent increase to values above the theoretical limit of eight electrons per BH_4^- will be discussed in Section 3.2.3, with the DEMS results. Here we only note that in this potential range also contributions from double-layer charging are highest, and that the Faradaic current measurements (Fig. 3) indicate significant kinetic limitations, as evidenced by the slow increase of the Faradaic current. The less pronounced decay at higher potentials compared to Pt/C can be attributed to the synergistic effects,

which were discussed already in detail in Section 3.1.3. Similar trends in the calculated number of electrons per borohydride ion in the BOR as for the AuPt/C catalyst, with synergistic contributions from both components, were reported also for a set of Pd/C, Au/C and a series of Au_xPd_y/C thin-film catalyst electrodes [37].

In summary, the evaluation of the electron transfer numbers via the Koutecky-Levich formalism fully confirmed our conclusions based on the maximum reaction currents and on the potential dependent hydrogen formation [32] of a predominant complete borohydride oxidation on the Pt containing nanoparticle catalysts in the potential region up to the onset of Pt-OH/Pt-O formation, while at higher potentials and for the Au/C catalyst over the entire potential region where the BOR is active, incomplete oxidation prevails.

3.2. DEMS measurements

In this section, we present and briefly discuss potentiodynamic DEMS measurements performed under continuous electrolyte flow conditions in a thin-layer flow cell, which are similar to those reported earlier for the BOR using isotope labelled BD_4^- species and were also recorded under similar conditions [32], however, with normal borohydride. Comparison with the earlier data allows us to identify kinetic isotope effects in the kinetic currents, which because of the complex multistep reaction may differ also with potential. Furthermore, they allow a more direct comparison with the RDE data in Section 3.1 and with published data on the BOR using normal borohydride, because of the absence of possible kinetic isotope effects. In the discussion, we will therefore focus on differences with respect to the data in reference [32] and aspects, which had not been discussed in that earlier paper. This also includes the evaluation of the number of electrons transferred electrons per borohydride ion as a function of the potential from the measured Faradaic current and the hydrogen evolution rate.

3.2.1. DEMS measurements of the BOR on a Pt/C thin-film electrode

Measurements of the BOR on a Pt/C catalyst are presented in Fig. 5. Over a wide potential range, they show the base voltammetry features superimposed on the mass transport limited current (Fig. 5a). This fully agrees with previous DEMS measurements on the BOR on BD_4^- [32] and also with the general shape of the RDE measurements at low rotation rates (Fig. 1, solid lines), As discussed in Section 3.1.1, they exhibit a very steep onset of the reaction at oxidation at lower potential limit and a slow decay of the BOR current above 0.6 V. The distinct structures visible in the RDE measurements between 0.7 and 1.0 V are not resolved because of the much lower electrolyte transport. The simultaneously monitored m/z = 2 ion current (Fig. 5b) reveals rapidly increasing bulk evolution of H_2 at very low potentials, below 0.1 V, which by DEMS detection of H_2 during oxidation of isotope labeled borodeuteride was identified to result from water reduction [32]. Up to the PtO region, there is no measurable m/z = 2 ion current, which corresponds to the transfer of close to 8 electrons per borohydride ion derived from the Koutecky-Levich analysis of the RDE data (Fig. 4). Together with the onset of OH adsorption / PtO formation at 0.75 V (see base CV in Fig. S3), we find an increasing H_2 signal, which reaches its maximum at about 1.1 V and then decays slowly, similar to the Faradaic current in this region. Hence, while in the range between 0.75 and 1.1 V the decay in Faradaic current is at least partly due to a change in BOR selectivity (increasing contributions from incomplete borohydride oxidation), at higher potentials it seems to be mainly caused by other kinetic limitations, with little change in the selectivity. Also these trends agree fully with the results obtained for BD_4^- oxidation [32]. From those previous measurements, we also know that the H_2 signal in this potential range stems from the incomplete oxidation of BH_4^- and not from a reaction involving decomposition of water. Our present results are consistent also with those of a comparable DEMS study of the BOR over a Pt/C catalyst in a flow cell [26], which showed an ill-resolved slight increase of H_2 evolution in the PtO region and a H_2 evolution increase at low

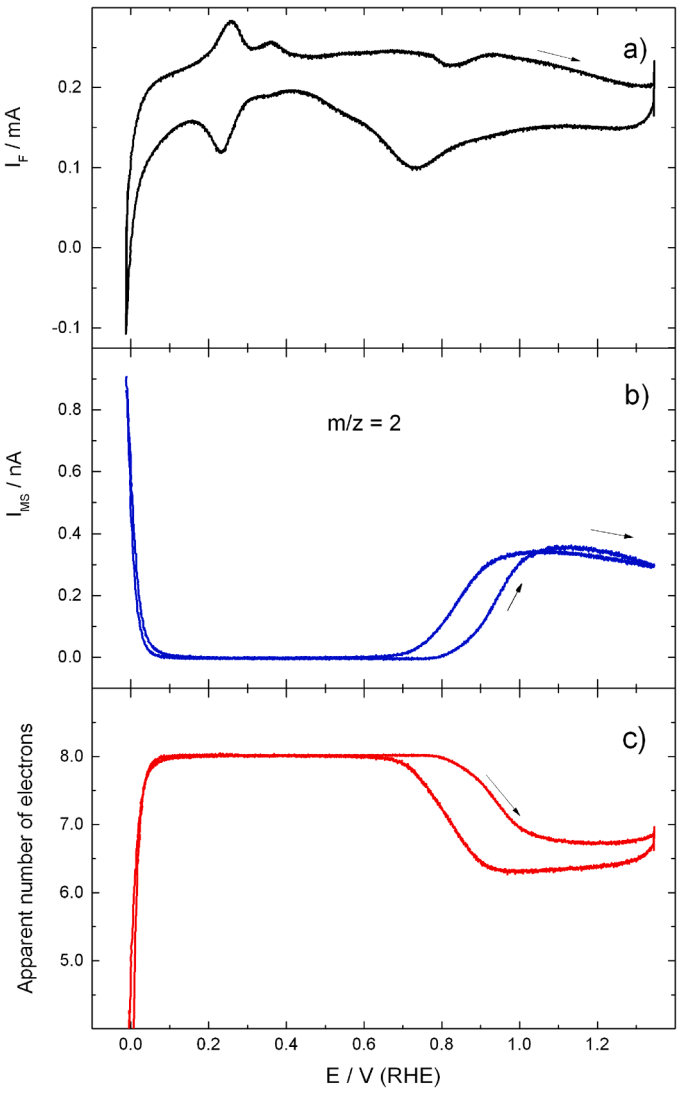

Fig. 5. DEMS measurement of the BOR over a Pt/C thin-film electrode. a) CV, b) mass spectrometric CV (MSCV) and c) apparent electron number per borohydride oxidation. Electrolyte: 0.1 mM $NaBH_4$ in 0.5 M NaOH, potential scan rate: 10 mV s^{-1}, electrolyte flow rate: 3 µl s^{-1}, metal loading: 40 µg cm^{-2}, room temperature. The related base CV is presented in Fig. S3.

potentials, which those authors attributed to the reduction of water. The much better resolution of the H_2 signal and the resulting excellent signal-to-noise ratio in the present measurements are due to the use of the liquid nitrogen trap at the inlet to the mass spectrometer chamber. This strongly reduces the water vapor pressure at the ionization chamber of the mass spectrometer and thus the resulting background of the fragment at m/z = 2 from water ionization, by about two orders of magnitude. This allows a highly sensitive detection and quantification of the m/z = 2 signal variation even at very small H_2 formation rates.

Following the approach used in [26], we have calculated the number of electrons per borohydride ion consumed $n_{e-/BH4-}$ from the measured Faradaic current I_F via Eq. (3)

$$n_{e-/BH4-} = (8' I_F)/(I_F + I_{H2}), \quad (3)$$

where the equivalent current for the H_2 evolution (I_{H2}) is calculated from the m/z = 2 ion current via the separately measured calibration constant (K*) for the two-electron hydrogen evolution in the supporting electrolyte $K^* = (2 \times I_{m/z=2}) / I_F$ [41]. The resulting apparent number of electrons released per one borohydride ion is shown as function of the potential in Fig. 5c. Note that the use of an 'apparent number of

electrons' refers to the fact that at low potentials we cannot distinguish between contributions from the BOR and the H_2 evolution reaction (HER) to the measured Faradaic current I_F, which can lead to severe underestimates of the electron number or even negative values for the BOR in this potential region. Considering also the contributions from capacitive and adsorption/desorption currents, as indicated by the base voltammogram of Pt/C (see Fig. S3), we find a transfer of approximately eight electrons per BH_4^- over a wide potential range, from ca. 0.2 to about 0.8 V, in good agreement with the values derived from the RDE measurements (Fig. 4a). Also Pasqualeti et al. reported a broad plateau of 8 electrons per borohydride in the double-layer region [26]. At lower potentials, below about 0.1 V, the electron number decays to zero (Fig. 5a), which can be explained as a result of the counteracting contributions from the BOR and the increasing H_2 evolution reaction (HER) at potentials close to the open circuit potential [26]. Contributions from the BOR in this potential region, despite an apparently zero or even negative measured current, are supported also by the observation of HD and D_2 when using deuterated borohydride [32], in addition to H_2. At potentials below the apparent onset potential of the BOR, the contribution from the electrochemical reduction of water is dominant.

The number of electrons transferred per BH_4^- decreases also at potentials positive of 0.8 V, reaching about 6.5 electrons per borohydride at ca. 1.0 V, and then remains nearly constant over the whole PtO region, up to the upper potential limit of 1.36 V (Fig. 5c). The general trend resembles that in Fig. 4a, where the number of electrons also started to decay at about 0.8 V, reaching a value of about 6 electrons per BH_4^- oxidation. Hence, both measurements indicate a distinct change in BOR selectivity towards incomplete oxidation at potentials positive of 0.8 V, on the OH_{ad} covered / oxidized Pt surface. Our results agree rather well also with the decay of the electron transfer number from eight to ca. seven in the PtO region reported by Pasqualeti et al. [26].

Finally, combining these data with those we had reported previously for the BOR of deuterated borohydride [32], allows us to assess kinetic isotope effects (KIEs). These are evaluated from the kinetic BOR currents in Fig. 5a, which are derived from the measured Faradaic currents assuming that under these transport conditions the mass transport limited current is identical to the maximum current in Fig. 5 of about 0.2 mA. The kinetic currents r_H and r_D as well as the resulting kinetic isotope effect KIE = r_{BH4} / r_{BD4} are plotted in Fig. S6. The low values of the r_{BH4} / r_{BD4} ratio of between 1 and at most 1.5 at all relevant potentials point to a secondary KIE, which indicates that B-H bond breaking or a subsequent product-determining step in the BOR on Pt/C do not represent the rate limiting step [65]. Secondary KIEs are observed, e.g., for a change in the steric environment, when the atom bound to the H/D undergoes rehybridization, e.g., from sp^3 to sp^2 or vice versa [65]. Furthermore, KIEs do not result in significant modifications of the BOR characteristics on Pt/C.

In summary, these DEMS measurements revealed considerable changes in the BOR selectivity of Pt/C with potential, with a high selectivity for the complete oxidation in the potential region up to the onset of Pt-OH/Pt-O formation and considerably lower selectivity in the PtO potential region. This was indicated by the observation of H_2 in the latter potential region and quantified by calculating the electron transfer number per BH_4^- based on the H_2 formation current. In the low-potential region, close to the onset of the BOR, these numbers are lowered by contributions from the HER and therefore not characteristic for the BOR. In combination with previous data, they allowed us to derive kinetic isotope effects, which revealed that B-H bond breaking does not represent the rate limiting step in the BOR on this catalyst. This finding agrees well also with conclusions in previous density functional theory (DFT) based calculations [66] and in a kinetic modeling study [67].

3.2.2. DEMS measurements of the BOR on a Au/C thin-film electrode

Similar DEMS measurements of the BOR on a Au/C catalyst (Fig. 6) show no activity up to ca. 0.2 V, in good agreement with the RDE data (Fig. 2) and our previous data obtained for borodeuteride oxidation on

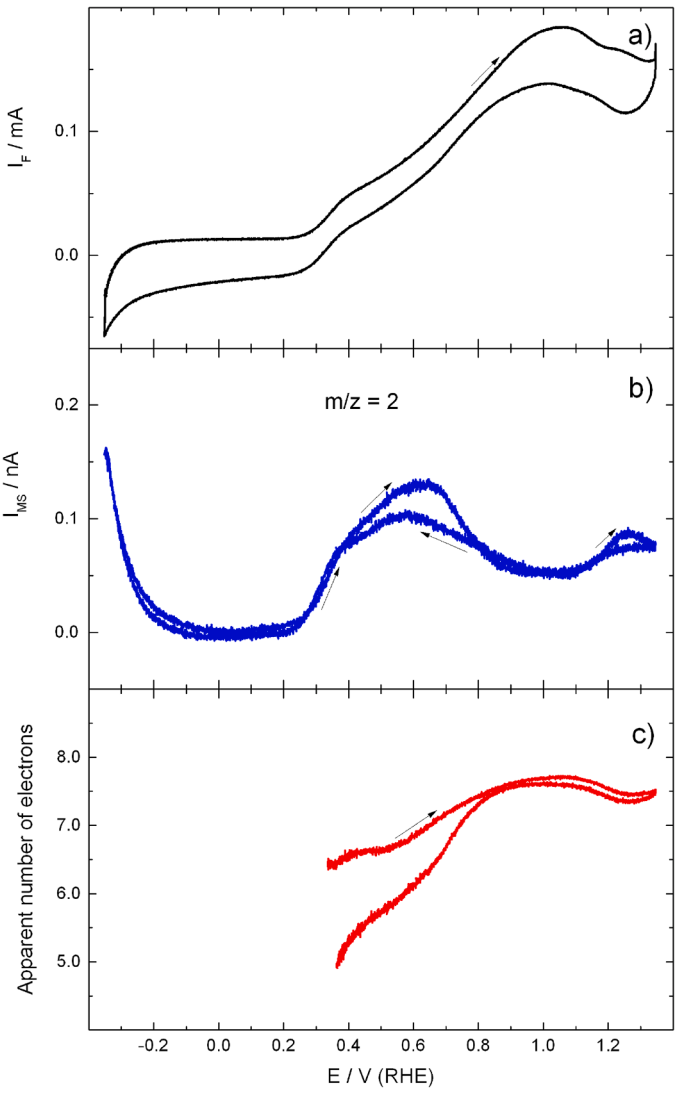

Fig. 6. a) CV, b) MSCV and c) the apparent number of electrons transferred per borohydride oxidation for the BOR over a Au/C (ZSW, 8.0 wt.%) thin-film electrode. Electrolyte: 0.1 mM $NaBH_4$ in 0.5 M NaOH, potential scan rate: 10 mV s^{-1}, electrolyte flow rate: 3 µl s^{-1}, metal loading: 15 µg cm^{-2}, room temperature. The related base CV is presented in Fig. S4.

this catalyst [32]. This also agrees with predictions based on DFT and microkinetic modeling [10]. After the onset of oxidation, the Faradaic current passes an ill-resolved shoulder at ca. 0.4 V and increases further until reaching the maximum at around 1.0 V. At higher potentials, it decreases again. In the negative-going scan, the current response essentially reproduces that in the positive-going scan, considering the superimposed pseudo-capacitive features of the Au/C base CV (see Fig. S4), and changes into a reduction current close to the low potential limit. The latter is associated with the evolution of hydrogen, as can be seen from the increase of m/z = 2 ion current at potentials below -0.1 V (Fig. 6b). Going to higher potentials, the m/z = 2 ion current sets in more positive of 0.2 V, passes a broad asymmetric peak with a distinct shoulder, which corresponds to an ill-resolved shoulder of the Faradaic current at ca. 0.4 to 0.5 V, and decays to lower values at potentials positive of 0.6 V. This latter decay is in contrast to the increase of the Faradaic current in this potential range. The peak of the m/z = 2 ion current in the potential range 0.3 to 0.6 V is related to H_2 formation during borohydride oxidation, as evidenced using deuterated borohydride in [32]. (Here it should be noted that in reference [32] we used a different correction for the time delay between Faradaic current and

mass spectrometric signal, which for this catalyst resulted in a more pronounced potential separation between positive-going and negative-going scan and in a more pronounced hysteresis in the H_2 signal at about 0.25 V. Using the same correction as in the present work, the shapes are identical.) In contrast, H_2 formation at low potentials originates from the reduction of water. The opposite trends of the Faradaic and m/z = 2 ion current responses at potentials ≥ 0.6 V clearly suggest a potential-dependent change in the BOR selectivity of the Au/C electrode. Comparable DEMS measurements of borohydride oxidation on a Au/C catalyst in a thin-layer DEMS cell by Pasqualeti et al. [26] also showed a decrease of the H_2 evolution rate prior to AuO formation, but down to the background level, while in our measurements it decreases only by less than 50 %. We explain this difference by experimental problems in the measurement of the m/z = 2 signal in that earlier work. Furthermore, those authors had assigned the H_2 evolution at the onset of the BOR to a catalytic hydrolysis of borohydride [26], which is in contrast to the absence of hydrogen evolution at a Au/C catalyst under open-circuit conditions, upon open circuiting a pre-oxidized Au/C catalyst [32,37]. Instead, it must be due to incomplete borohydride oxidation, which is reasonable also when considering that gold is not active for the hydrogen oxidation (Fig. 2 and [48]).

Finally, we would like to note that from the present observations of a considerable reaction current and H_2 formation in the oxide potential region alone we would not be able to separate between a reaction proceeding via the electrooxidation of Au and subsequent chemical reaction between Au oxide and borohydride on the hand and direct electrocatalytic oxidation of borohydride on the other hand. In a continuous reaction, both would result in the same number of electrons transferred. Considering, however, that reduction of a pre-formed Au surface oxide was observed in open circuit transients with the release of D_2 from the D-labeled borohydride and reduction of the oxide [32], we conclude that the first pathway will at least contribute to the measured reaction current and H_2 evolution in the oxide potential region.

A plot of the apparent number of electrons transferred per borohydride oxidation over a Au/C electrode (Fig. 6c) shows an initial value of about 6.5 in the positive-going scan, indicative of an incomplete (partial) oxidation of borohydride with the release of H_2 and incomplete oxidation intermediates (Eq. (2)). This number is somewhat higher than the about four electrons obtained via the Koutecki-Levich analysis (Fig. 4). Reasons for this discrepancy will be discussed below. With increasing potential, this number increases, reaching a maximum value of close to eight at a potential of 1 V. This increase in electron number results from an increase of the Faradaic current in combination with the hydrogen formation rate (Fig. 6a and b). This increase agrees with the trend in the RDE measurements (Fig. 4b) and also with results of rotating ring-disk experiments, which showed an increase of the ring current in this potential range. This was associated with the oxidation of the reaction intermediates in this potential region (note that in those experiments the Au ring was set to a potential where borohydride oxidation is inhibited) [18,26,43]. It also fits to the observation of bands attributed to adsorbed reaction intermediates in SERS measurements [10]. At higher potentials, the electron number decreases slowly, by about 0.3 e^-, which also agrees with the trend in the Faradaic current. Thus, under present reaction conditions, complete oxidation is hardly reached. Even at potentials around 1 V, where the electron number reaches its maximum, there is still measurable H_2 formation, reflecting contributions from incomplete oxidation. It should be noted that this statement is highly reliable, since H_2 formation (above the background level in the mass spectrometer) can be measured with high sensitivity. In the negative-going scan, the electron number largely follows this trend, except for a slight displacement to lower numbers due to the capacitive contributions. Only at potentials below 0.8 V, it deviates increasingly to lower electron numbers.

Comparing these DEMS-based data with the RDE-based data in Fig. 4b, we find a similar trend with potential, while the absolute numbers are lower in Fig. 4b. The lower electron numbers in the RDE measurements are caused by the much higher electrolyte transport in this measurement, which is evidenced also by the much higher measured reaction current. This favors the off-transport of incomplete oxidation products as compared to re-adsorption and further reaction, and thus results in a tendency towards incomplete oxidation (lower selectivity for complete oxidation) and therefore a lower number of electrons transferred per BH_4^- consumed in the RDE experiment [45]. Using Pt/C catalyst layers of different thickness, comparable effects had also been reported for the BOR by Freitas et al. [21].

Comparable effects are held responsible also for the increasing deviation in the number of electrons transferred between positive-going and negative-going scan at potentials below 0.8 V. This is due to increasing contributions from the base CV to the measured current, in particular from double layer charging, which will modify the measured current accordingly. Such effects, which are generally present, become important in particular at low measured currents, as they are obtained, e.g., for the Au/C catalyst electrode for potentials < 0.8 V (see Fig. 6a and 6c).

A similar evaluation of the kinetic isotope effect as described before for the BOR on Pt/C is plotted in Fig. S6. Also in this case, we find low values for the r_{BH4} / r_{BD4} ratio of between 1 and at most 1.5 at all relevant potentials, indicative of a secondary KIE where B-H bond breaking does not represent the rate limiting step or a subsequent product-determining step. In this case, contributions from the HER or HOR in the onset region of the BOR can be neglected, different from Pt/C. Nevertheless, also on this catalyst, KIEs do not result in significant modifications of the BOR characteristics.

In summary, these DEMS measurements with their high sensitivity and low noise in the m/z=2 signal provided a detailed picture of the potential dependent changes of the BOR selectivity of the Au/C catalyst for incomplete vs. complete oxidation, with rather complex variations in the potential dependent low selectivity. Similar to Pt/C, the Au/C catalyst is active for the BOR also in the Au oxide region, in the presence of an OH/O cover layer, though with a distinctly different potential dependence. The low activity of the Au/C catalyst for complete BOR oxidation agrees well also with its inactivity in the HOR. Finally, a similar evaluation of the kinetic isotope effects as described for Pt/C revealed that also in this case B-H bond breaking does not represent the rate limiting step in the BOR on Au/C (see also refs. [66,67].

3.2.3. *DEMS measurements of the BOR on a AuPt/C thin-film electrode*

The results of similar DEMS measurements performed on a AuPt/C electrode are presented in Fig. 7. The CV (Fig. 7a) exhibits similar characteristics as found in the RDE measurements (Fig. 3), with a low onset potential, a broad current maximum at about 0.6 – 1.0 V and a later decay. The early BOR onset resembles the behavior of Pt/C (Figs. 1 and 5), while the later decay of the BOR current with considerable currents in the oxide region is more characteristic for Au/C (Figs. 2 and 6). Based on the featureless, low m/z = 2 signal, H_2 formation is fully suppressed over a wide potential range, between 0.1 and 0.8 V, similar to the reaction on Pt/C (Fig. 5), but different from that on the Au/C electrode (Fig. 6). Hence, H_2 oxidation is highly efficient in this potential range, indicating that H_{ad} adsorbing on Au sites can easily surface diffuse to Pt or mixed sites that are active for the HOR (see also Section 3.1.3). Furthermore, the evolution of H_2 at potentials positive of 0.3V, which occurs on the Au/C electrode (Fig. 6), is largely missing over the AuPt/C catalyst. Most simply, this can also be explained by a spill-over of the H_{ad} formed at gold sites to the HOR-active Pt sites, where it is immediately oxidized. On the other hand, the increase in the m/z = 2 ion current in the oxide region is less pronounced on the AuPt/C electrode than on the Pt/C electrode (Fig. 5). Together with the observation of a later onset of the Pt oxidation (see base CV in Fig. S5), this indicates that PtO formation is somewhat hindered when Pt is surface alloyed with Au [55] (see also our discussion in Section 3.1.3 and below). Furthermore, both CV and MSCV closely resemble those obtained for borodeuteride oxidation on this catalyst in their characteristic features

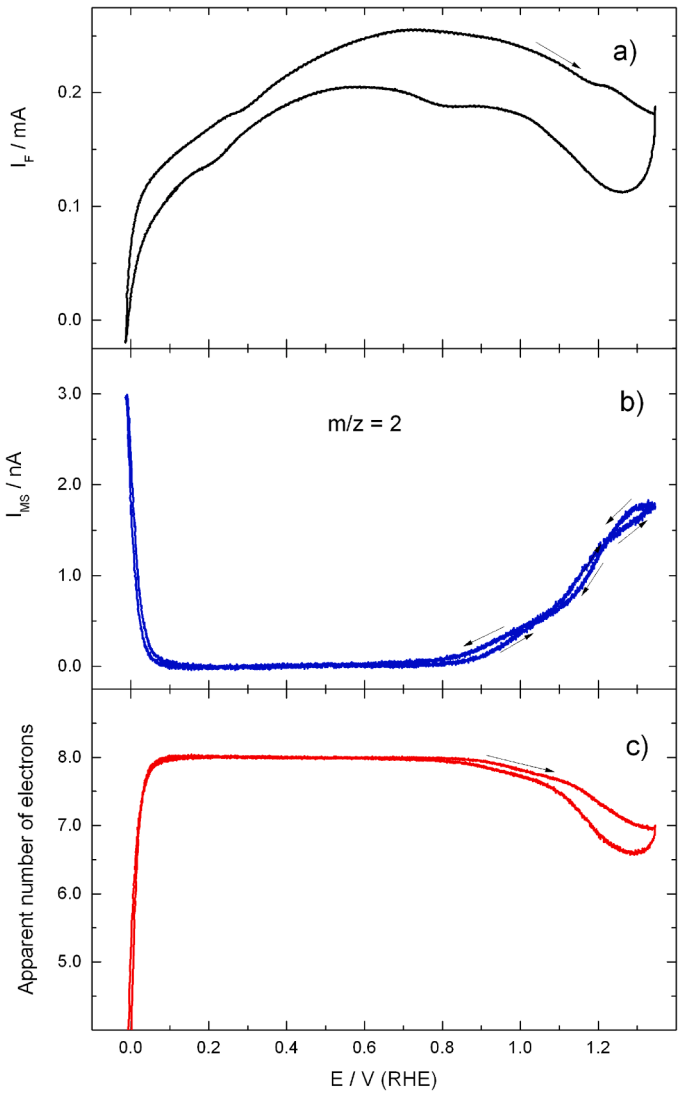

Fig. 7. CV, MSCV and the apparent electron number per borohydride oxidation for the BOR over a AuPt/C (ZSW, 25 wt.%) thin-film electrode. Electrolyte: 0.1 mM $NaBH_4$ in 0.5 M NaOH, potential scan rate: 10 mV s^{-1}, electrolyte flow rate: 3 µl s^{-1}, metal loading: 50 µg/cm^{-2}, room temperature. The related base CV is presented in Fig. S5.

[32], indicating that kinetic isotope effects do not result in significant changes in their characteristic features. The latter measurements also indicated that at low potentials (< 0.1 V) H_2 formation is dominated by water reduction (H_2, m/z = 2), with small amounts from borodeuteride oxidation even at the onset of the BOR, as evidenced by small signals of HD (m/z = 3) and D_2 (m/z = 4). At high potentials (> 0.9 V), in contrast, deuterium formation from incomplete borodeuteride oxidation occurs over the oxide covered catalyst.

The trend of a more Pt-like (not Pt identical!) behavior in the lower potential region, up to 0.6 V, and a more Au-like or better Au oxide like behavior in the oxide region is reflected also by the apparent number of transferred electrons (Fig. 7c). This shows a rapid increase at potentials up to 0.1 V, followed by a constant value of around eight electrons between 0.1 and 0.8 V, which closely resembles the behavior observed for the Pt/C catalyst electrode. The only major difference compared to Pt/C is the less pronounced hysteresis between positive-going and negative-going scans in the potential range around the onset of oxide formation on the AuPt/C catalyst electrode. Obviously, in this range the overpotentials for Pt oxide formation and Pt oxide reduction, respectively, are reduced by interaction with Au, leading to this decay in hysteresis. Similar effects had been reported also by Tang et al. for methanol oxidation on AuPt nanoparticle electrodes [68]. In the oxide region, in contrast, it resembles more the trend obtained for the Au/C catalyst, with a continuous decrease rather than a steep decrease followed by a constant low value as obtained for Pt/C. Most likely, oxidation of borohydride on Au and Au oxide sites is significantly faster than reaction on Pt oxide sites.

Comparison of the number of electrons transferred during reaction in Fig. 7c with the data derived from RDE measurements (Fig. 4c) reveals similar trends for potentials positive of 0.8 V. Differences appear, however, at lower potentials, between the onset of the reaction and that value, where the DEMS data indicate complete oxidation with eight electrons per BH_4^- consumed, while the RDE show a continuous increase to higher numbers with decreasing potential. As already mentioned in the discussion in Section 3.1.4, values of above 8 electrons per BH_4^- are unphysical for the BOR, as this represents the maximum number of electrons released during complete oxidation of borohydride. The DEMS data support our tentative explanation in Section 3.1.4 that the higher electron numbers derived from the Koutecky-Levich (KL) analysis of the RDE data in this potential range are the result of an artifact in that analysis, caused either by the contributions from the base CV in the reaction current or by a change in selectivity with increasing transport. Interestingly, this is also the potential region where the measured reaction current is strongly affected by kinetic limitations, as indicated by its rather slow increase of the reaction current after the onset of the reaction (Fig. 3), much slower than observed for the Pt/C electrode (Fig. 1).

The evaluation of kinetic isotope effects (Fig. S8) revealed that also for the BOR on AuPt/C the r_{BH4} / r_{BD4} ratio is between 1 and at most 1.5 at all relevant potentials, indicative of a secondary KIE. We would like to note that in this case the potential dependence of the KIE in the positive-going scan seems to follow the general trend in the Faradaic current, although a detailed mechanistic explanation is still missing. Nevertheless, also for this catalyst B-H bond breaking does not represent the rate limiting step or a subsequent product-determining step, and KIEs have no significant impact on the BOR characteristics.

In total, the DEMS measurements of the BOR on the AuPt/C catalyst electrode confirmed the synergistic behavior of this catalyst concluded already from the RDE measurements, with a more Pt-like, but not Pt-identical behavior in the lower potential regime, where the Au/C catalyst is inactive for the BOR and hydrogen evolution. In the oxide region, in contrast, its behavior is more Au-like, but not Au-identical. Finally, the evaluation of the kinetic isotope effects revealed that B-H bond breaking or B-H bond making do not represent the rate-limiting step in the BOR on AuPt/C.

Finally we would like to comment on the role of the oxides on the above catalysts in the BOR, which was addressed in detail in our previous contribution [32]. In a set of DEMS measurements, starting with a catalyst pre-oxidized at 1.04 V, followed by open-circuiting, and simultaneously monitoring the rest potential of the electrode and the H_2, HD and D_2 formation in a thin-layer DEMS flow cell, we found that the metal oxides can be reduced by reaction with borohydride, with no evolution of D_2 (complete D-borohydride oxidation) for the Pt-containing catalysts. In contrast, there is release of D_2 (incomplete oxidation) during the potentiometric transient upon the reduction of Au oxide by borodeuteride. Such a difference in the selectivity of borohydride oxidation even under open-circuit conditions reflects also the inability of a gold electrode to oxidize hydrogen. Based on these results, electrooxidation of borohydride can at least in principle not only proceed via direct electrooxidation along Eqs. (1) or (2), but also by electrooxidation of the metal and subsequent reduction of the metal oxide by a chemical reaction between borohydride and the oxide. The relevance of this pathway shall be investigated in more detail in future.

4. Summary

Aiming at a more detailed understanding of the kinetics, mechanism and mass transport effects of/in the borohydride oxidation reaction (BOR), we have systematically studied this reaction in alkaline solution over structurally well-defined carbon-supported Pt/C, Au/C and AuPt/C catalysts. Employing rotating disk electrode (RDE) and differential electrochemical mass spectrometry (DEMS) measurements under controlled electrolyte transport conditions and using thin-film catalyst electrodes, we arrived at the following main insights and conclusions:

1. Systematic RDE measurements and comparison with the H_2 oxidation reaction revealed that for the Pt containing catalysts the mass transport limited current is (approximately) reached only at low transport conditions and in a limited potential range around 0.3 V for Pt/C. At higher transport conditions and at lower / higher potentials, kinetic limitations play an increasing role. Except for the oxide potential range, these limitations do not involve a change in selectivity, as evidenced by the absence of H_2 formation in this potential range, but must result from other kinetic limitations such as (partial) surface blocking. For the BOR on Au/C and on AuPt/C, the Faradaic currents are well below the mass transport limited current under all reaction condition. For Au/C, the kinetic limitations also leads to incomplete borohydride oxidation, which is indicated by the H_2 formation at all potentials.
2. Evaluation of the number of electrons transferred per borohydride ion oxidation via the Koutecky-Levich formalism revealed numbers close to 8 on the Pt/C and AuPt/C catalyst electrodes in the potential region from about 0.2 V up to the onset of oxide formation at about 0.8 V. For Pt/C, it starts to decay steeply at that potential, while for AuPt/C this decrease is much slower. This decay provides further support of a change in the BOR selectivity from complete oxidation to incomplete oxidation. For Au/C, the number of electrons transferred per BH_4^- varies between 4.1 and 5.5 in the RDE measurements. Thus incomplete oxidation prevails under these conditions, independent of the potential. Comparable trends were obtained from the evaluation of the total Faradaic current and the currents required for H_2 formation in the DEMS measurements, although under these conditions, at significantly slower electrolyte transport and therefore an increased tendency towards complete oxidation, the electron number is generally higher, between 5 and up to close to 8 at about 0.9 – 1.1 V.
3. For Pt-containing catalysts, the simultaneous BOR and H_2 evolution from water reduction result in effective Faradaic currents in the range around 0 V_{RHE}. Thus, BH_4^- oxidation is also possible in the range of low negative Faradaic currents, where the negative HER current overcompensates the still existing positive BOR current.
4. Highly sensitive differential electrochemical mass spectrometry measurements, applying a liquid nitrogen cold trap before the inlet to the ionization chamber of the mass spectrometer, allowed us to sensitively monitor H_2 formation even at low rates without interference with H_2 fragments from water vapor ionization. The absence of even small amounts of H_2 evolution down to the onset of water reduction at about 0.1 V confirms earlier reports of complete 8-electron oxidation of borohydride over Pt/C and AuPt/C catalysts. In the oxide region, the clear detection of significant amounts of H_2 formation indicates incomplete borohydride oxidation, arising from the interaction of borohydride with the metal oxides, which is in contrast to previous DEMS measurements [26]. In addition to the significant overpotential, the BOR over the Au/C catalyst is dominated by incomplete oxidation, as evidenced by the much lower electron transfer per borohydride and the H_2 evolution over the whole region where the BOR is active on this catalyst.
5. Comparison of the DEMS results with data reported earlier for the BOR of deuterated BD_4^- species [32] shows that there are no significant differences, indicating that kinetic isotope effects (KIEs) are small and do not vary much with potential. Quantitative evaluation of the potential dependent KIEs results in low values of the r_{BH4} / r_{BD4} ratio of between 1 and 1.5 at most for all catalysts and at all relevant potentials, indicating a weak secondary KIE. Accordingly, B-H bond breaking does not represent the rate-limiting step or a subsequent product determining step in the BOR on these catalysts.

As a general point, this work underlines the importance of measurements under high-transport conditions in model studies of technical fuel cell reactions, as they provide a relevant picture of the role of kinetic and transport limitations under technically relevant high transport reaction conditions.

CRediT authorship contribution statement

Zenonas Jusys: Writing – original draft, Visualization, Validation, Investigation, Formal analysis, Data curation, Conceptualization. **R. Jürgen Behm:** Writing – review & editing, Visualization, Resources, Project administration, Funding acquisition, Conceptualization.

Declaration of competing interest

The authors declare that they have no known competing financial interests or personal relationships that could have appeared to influence the work reported in this paper.

Acknowledgements

We dedicate this contribution to our long-time colleague and friend Professor Elena Savinova, with great respect for her many inspiring contributions to the field of electrochemistry in general and specifically electrocatalysis. This work was supported by the Brennstoffzellen-Allianz Baden-Württemberg (BzA-BW). We gratefully acknowledge Dr. L. Jörissen and Dipl. Chem. U. Riek, both Centre for Solar Energy and Hydrogen Research (ZSW), Ulm, Germany, for providing the Au/C and Au/Pt/C catalysts and for catalyst synthesis and characterization, respectively. This work contributes to the research performed at CELEST (Center for Electrochemical Energy Storage at Ulm and Karlsruhe). Open Access was enabled and organized by project DEAL.

Supplementary materials

Supplementary material associated with this article can be found, in the online version, at doi:10.1016/j.electacta.2024.145608.

Data availability

Data will be made available on request.

References

[1] C. Ponce de Leon, F.C. Walsh, D. Pletcher, D.J. Browning, J.B. Lakeman, Direct borohydride fuel cells, J. Power Sources 155 (2006) 172–181.
[2] I. Merino-Jiménez, C. Ponce de León, A.A. Shah, Walsh, Developments in direct borohydride fuel cells and remaining challenges, J. Power Sources 219 (2012) 339–357.
[3] R.M.E. Hjelm, C. Lafforgue, R.W. Atkinson III, Y. Garsany, R.O. Stroman, M. Chatenet, K. Swider-Lyons, Impact of the anode catalyst layer design on the performance of H_2O_2-direct borohydride fuel cells, J. Electrochem. Soc. 166 (2019) F1218–F1228.
[4] J.-H. Wee, A comparison of sodium borohydride as a fuel for proton exchange membrane fuel cells and for direct borohydride fuel cells, J. Power Sources 155 (2006) 329–339.
[5] J.-H. Wee, Which type of fuel cell is more competitive for portable application: direct methanol fuel cells or direct borohydride fuel cells? J. Power Sources 155 (2006) 329–339.
[6] S.J. Kim, J. Lee, K.J. Kong, C.R. Jung, I.-G. Min, S.-Y. Lee, H.-J. Kim, S.V. Nam, T.-H. Lim, Hydrogen generation system using sodium borohydride for operation of a 400 W-scale polymer electrolyte fuel cell stack, J. Power Sources 170 (2007) 412–418.

[7] U.B. Demirci, O. Akdim, J. Andrieux, J. Hannauer, R. Chamoun, P. Miele, Sodium borohydride hydrolysis as hydrogen generator: issues, state of the art and applicability upstream from a fuel cell, Fuel Cells 10 (2010) 335–350.

[8] R.A. Davis, E. Bromels, C.L. Kibby, BoronHydrides. III. hydrolysis of sodium borohydride in aqueous solution, J. Am. Chem. Soc. 84 (1962) 885–892.

[9] A. Oshchepkov, A. Bonnefont, G. Maranzana, E.R. Savinova, M. Chatenet, Direct borohydride fuel cells: a selected review of their reaction mechanisms, electrocatalysts, and influence of operating parameters on their performance, Current Opin. Electrochem. 32 (2022) 100883.

[10] G. Rostamikia, A.J. Mendoza, M.A. Hickner, M.J. Janik, First-principles based microkinetic modeling of borohydride oxidation on a Au(111) electrode, J. Power Sources 196 (2011) 9228–9237.

[11] P.-Y. Olu, C.R. Barros, N. Job, M. Chatenet, Electrooxidation of NaBH4in alkaline medium on well-defined Pt nanoparticles deposited onto flat glassy carbon substrate: evaluation of the effects of Pt nanoparticle size, interparticle distance, and loading, Electrocatal 5 (2014) 288–300.

[12] P.-Y. Olu, A. Bonnefont, M. Rouhet, S. Bozdech, N. Job, M. Chatenet, E. Savinova, Insights into the potential dependence of the borohydride electrooxidation reaction mechanism on platinum nanoparticles supported on ordered carbon nanomaterials, Electrochim. Acta 179 (2015) 637–646.

[13] G. Rostamikia M.J. Janik, Direct borohydride oxidation: mechanism determination and design of alloy catalysts guided by density functional theory, Energy Environ. Sci. 3 (2010) 1262–1274.

[14] G. Rostamikia M.J. Janik, First principles mechanistic study of borohydride oxidation over the Pt(111) surface, Electrochim. Acta 55 (2010) 1175–1183.

[15] M.C. Sison Escano, E. Gyenge, R.L. Arevalo, H. Kasai, Reactivity descriptors for borohydride interaction with metal surfaces, J. Phys. Chem. C 115 (2011) 19883–19889.

[16] E. Gyenge, Electrooxidation of borohydride on platinum and gold electrodes: implications for direct borohydride fuel cells, Electrochim. Acta 49 (2004) 965–978.

[17] M. Chatenet, F. Micoud, I. Roche, E. Chainet, J. Vondrák, Kinetics of sodium borohydride direct oxidation and oxygen reduction in sodium hydroxide electrolyte: Part II. O_2Reduction, Electrochim. Acta 51 (2006) 5452–5458.

[18] P. Krishnan, T.-H. Yang, S.G. Advani, A.K. Prasad, Rotating ring-disc electrode (RRDE) investigation of borohydride electro-oxidation, J. Power Sources 182 (2008) 106–111.

[19] B. Molina Concha M. Chatenet, Direct oxidation of sodium borohydride on Pt, Ag and alloyed Pt–Ag electrodes in basic media Part II. carbon-supported nanoparticles, Electrochim. Acta 54 (2009) 6130–6139.

[20] M. Chatenet, F.H.B. Lima, E.A. Ticianelli, Gold Is not a faradaic-efficient borohydride oxidation electrocatalyst: an online electrochemical mass spectrometry study, J. Electrochem. Soc. 157 (2010) B697–B704.

[21] K.S. Freitas, B.M. Concha, E.A. Ticianelli, M. Chatenet, Borohydride oxidation on Pt-Based electrodes: evidence of residence time effect on the reaction onset and faradaic efficiency, ECS Trans 33 (2010) 1693–1699.

[22] B. Molina Concha, M. Chatenet, E.A. Ticianelli, F.B.H. Lima, In situ infrared (FTIR) study of the mechanism of the borohydride oxidation reaction on smooth Pt electrode, J. Phys. Chem. C 115 (2011) 12439–12447.

[23] F.B.H. Lima, A.M. Pasqualeti, M.Belen Molina Concha, M. Chatenet, E.A. Ticianelli, Borohydride electrooxidation on Au and Pt electrodes, Electrochim. Acta 84 (2012) 202–212.

[24] A. Ignaszak, D.C.W. Kannangara, V.W.S. Lam, E.L. Gyenge, Borohydride electro-oxidation on gold investigated by electrochemical quartz crystal microbalance, J. Electrochem. Soc. 160 (2013) H47–H53.

[25] P.-Y. Olu, F. Deschamps, G. Caldarella, M. Chatenet, N. Job, Investigation of platinum and palladium as potential anodic catalysts for direct borohydride and ammonia borane fuel cells, J. Power Sources 297 (2015) 492–503.

[26] A.M. Pasqualeti, P.-Y. Olu, M. Chatenet, F.H.B. Lima, Borohydride electrooxidation on carbon-supported noble metal nanoparticles: insights into hydrogen and hydroxyborane formation, ACS Catal 5 (2015) 2778–2787.

[27] V. Briega-Martos, E. Herrero, J.M. Feliu, Borohydride electro-oxidation on Pt single crystal electrodes, Electrochem. Commun. 51 (2015) 145–147.

[28] V.L. Oliveira, E. Sibert, Y. Soldo-Olivier, E.A. Ticianelli, M. Chatenet, Investigation of the electrochemical oxidation reaction of the borohydride anion in palladium layers on Pt(111), Electrochim. Acta 209 (2016) 360–368.

[29] P.Y. Olu, N. Job, M. Chatenet, Evaluation of anode (Electro)Catalytic materials for the direct borohydride fuel cell: methods and benchmarks, J. Power Sources 327 (2016) 235–257.

[30] G. Braesch, A. Bonnefont, V. Martin, E.R. Savinova, M. Chatenet, Borohydride oxidation reaction mechanisms and poisoning effects on Au, Pt and Pd bulk electrodes: from model (Low) to direct borohydride fuel cell operating (High) concentrations, Electrochim. Acta 273 (2018) 483–494.

[31] M.C. Sison Escaño, R.L. Arevalo, E. Gyenge, H. Kasai, Electrocatalysis of borohydride oxidation: a review of density functional theory approach combined with experimental validation, J. Phys.: Condens. Matter 26 (2014) 353001 (1)-353001(14).

[32] Z. Jusys R.J. Behm, Borohydride electrooxidation over Pt/C, AuPt/C and Au/C catalysts: partial reaction pathways and mixed potential formation, Electrochem. Commun. 60 (2015) 9–12.

[33] A. Tegou, S. Armyanov, A. Valova, O. Steenhaut, A. Hubin, G. Kokkinidis, S. Sotiropoulos, Mixed platinum–gold electrocatalysts for borohydride oxidation prepared by the galvanic replacement of nickel deposits, J. Electroanal. Chem. 634 (2009) 104–110.

[34] E. Gyenge, M. Atwan, D. Northwood, Electrocatalysis of borohydride oxidation on colloidal Pt and Pt-Alloys (Pt-Ir, Pt-Ni, and Pt-Au) and application for direct borohydride fuel cell anodes, J. Electrochem. Soc. 153 (2006) A150.

[35] X. Geng, H. Zhang, Y. Ma, H. Zhong, Borohydride electrochemical oxidation on carbon-supported pt-modified Au nanoparticles, J. Power Sources 195 (2010) 1583–1588.

[36] S.U. Karabiberoglu, L. Pelit, B. Gelmez, Z. Dursun, Electrocatalytic oxidation of sodium borohydride on metal Ad-atom modified Au(111) single crystal electrodes in alkaline solution, Int. J. Hydrogen Energy 36 (2011) 12678–12685.

[37] M. Simoes, S. Baranton, C. Coutanceau, Electrooxidation of sodium borohydride at Pd, Au, and Pd_xAu_{1-x}Carbon-supported nanocatalysts, J. Phys. Chem. C 113 (2009) 13369–13376.

[38] T.J. Schmidt, H.A. Gasteiger, G.D. Stäb, P.M. Urban, D.M. Kolb, R.J. Behm, Characterization of high-surface area electrocatalysts using a rotating disk electrode configuration, J. Electrochem. Soc. 145 (1998) 2354–2358.

[39] Y.-C. Lu, C. Xu, H.A. Gasteiger, S. Chen, K. Hamad-Schifferli, Y. Shao-Horn, Platinum - gold nanoparticles: a highly active bifunctional electrocatalyst for rechargeable lithium - air batteries, J. Am. Chem. Soc. 132 (2010) 12170–12171.

[40] Z. Jusys, H. Massong, H. Baltruschat, A new approach for simultaneous DEMS and EQCM: electro-oxidation of adsorbed CO on Pt and Pt-Ru, J. Electrochem. Soc. 146 (1999) 1093–1098.

[41] O. Wolter J. Heitbaum, The adsorption of CO on a porous pt-electrode in sulfuric acid studied by DEMS, Ber. Bunsenges. Phys. Chem. 88 (1984) 6–10.

[42] V.G. Levich, Physicochemical Hydrodynamics, Prentice Hall, Eaglewood Cliffs, NJ, 1962.

[43] D.A. Finkelstein, N.D. Mota, J.L. Cohen, H.D. Abruna, Rotating disk electrode (RDE) investigation of $BH_4^-$and BH_3OH^-electro-oxidation at pt and au: implications for BH_4^-fuel cells, J. Phys. Chem. C 113 (2009) 19700–19712.

[44] W. Sheng, H.A. Gasteiger, Y. Shao-Horn, Hydrogen oxidation and evolution reaction kinetics on platinum: acid Vs alkaline electrolytes, J. Electrochem. Soc. 157 (2010) B1529.

[45] Y.E. Seidel, A. Schneider, Z. Jusys, B. Wickman, B. Kasemo, R.J. Behm, Mesoscopic mass transport effects in electrocatalytic processes, Faraday Discuss. 140 (2008) 167–184.

[46] G. Parrour, M. Chatenet, J.P. Diard, Electrochemical impedance spectroscopy study of borohydride oxidation reaction on gold - towards a mechanism with two electrochemical steps, Electrochim. Acta 55 (2010) 9113–9124.

[47] M. Chatenet, M.B. Molina-Concha, J.P. Diard, First insights into the borohydride oxidation reaction mechanism on gold by electrochemical impedance spectroscopy, Electrochim. Acta 54 (2009) 1687–1693.

[48] E.G. Mahoney, W. Sheng, Y. Yan, J.G. Chen, Platinum-modified gold electrocatalysts for the hydrogen oxidation reaction in alkaline electrolytes, Chem. Electro. Chem. 1 (2014) 2058–2063.

[49] W. M. H. Sachtler, in *Handbook of Heterogeneous Catalysis*, G. Ertl, H. Knözinger, and J. Weitkamp, Eds. (VCH-Wiley, Weinheim, 1997), Vol. 3.

[50] Y. Soma-Noto W.M.H. Sachtler, Infrared spectra of carbon monoxide adsorbed on supported palladium and palladium-silver alloys, J. Catal. 32 (1974) 315–324.

[51] Y.L. Lam, J. Criado, M. Boudart, Enhancement by inactive gold of the rate of the H_2-O_2reaction on active palladium: a ligand effect, Nouv. J. Chim. 1 (1977) 461–466.

[52] M. Mavrikakis, B. Hammer, J.K. Nørskov, Effect of strain on the reactivity of metal surfaces, Phys. Rev. Lett. 81 (1998) 2819–2822.

[53] R.J. Behm, A. Groß, The chemistry of bimetalic surfaces - evolution of an atomic-scale picture, Surf. Sci. 754 (2025) 122677.

[54] A. Ruban, B. Hammer, P. Stoltze, H.L. Skriver, J.K. Nørskov, Surface electronic structure and reactivity of transition and noble metals, J. Mol. Catal. A 115 (1997) 421–429.

[55] A. Bergbreiter, O.B. Alves, H.E. Hoster, Entropy effects in atom distribution and electrochemical properties of Au_xPt_{1-x}/Pt(111) surface alloys, ChemPhysChem 11 (2010) 1505–1512.

[56] M. Eyrich, T. Diemant, H. Hartmann, J. Bansmann, R.J. Behm, Interaction of CO with structurally well-defined monolayer PtAu/Pt(111) surface alloys, J. Phys. Chem. C 116 (2012) 11154–11165.

[57] Y. Gohda A. Groß, Structure-reactivity relationships for bimetallic electrodes: Pt overlayers and PtAu surface alloys on Au(111), J. Electroanal. Chem. 607 (2007) 47–53.

[58] P. Sabatier, La Catalyse en Chimie Organique, Librairie Polytechnique Béranger, Paris, 1913.

[59] M.S. Ozório, M.F. Nygaard, A.S. Petersen, R.J. Behm, J. Rossmeisl, Self-induced long-range surface strain improves oxygen reduction reaction, J. Catal. 433 (2024) 115484.

[60] G. Denuault, M.V. Mirkin, A.J. Bard, Direct determination of diffusion coefficients by chronoamperometry at microdisk electrodes, J. Electroanal. Chem. Interfacial Electrochem. 308 (1991) 27–38.

[61] M. Chatenet, M.B. Molina-Concha, N. El-Kissi, G. Parrour, J.P. Diard, Direct rotating ring-disk measurement of the sodium borohydride diffusion coefficient in sodium hydroxide solutions, Electrochim. Acta 54 (2009) 4426–4435.

[62] M.J. Tham, R.D.J. Walker, K.E. Gubbins, Diffusion of oxygen and hydrogen in aqueous potassium hydroxide solutions, J. Phys. Chem. 74 (1970) 1747–1751.

[63] M. Schalenbach, A.R. Zeradjanin, O. Kasian, S. Cherevko, K.J.J. Mayrhofer, A perspective on low-temperature water electrolysis - challenges in alkaline and acidic technology, Int. J. Electrochem. Sci. 13 (2018) 1173–1226.

[64] P. Habibi, A. Rahbari, S. Blazquez, C. Vega, P. Dey, T.J.H. Vlugt, O.A. Moultos, A new force field for $oh^-$for computing thermodynamic and transport properties of $H_2$and O_2in aqueous NaOH and KOH solutions, J. Phys. Chem. B 126 (2022) 9376–9387.

[65] A. Streitwieser, Molecular Orbital Theory for Organic Chemists, John Wiley & Sons, New York, 1961.
[66] G. Rostamikia M.J. Janik, First principles mechanistic study of borohydride oxidation over the Pt(111) surface, Electrochimica Acta 55 (2010) 1175–1183.
[67] P.Y. Olu, A. Bonnefont, G. Braesch, V. Martin, E.R. Savinova, M. Chatenet, Influence of the concentration of borohydride towards hydrogen production and escape for borohydride oxidation reaction on pt and au electrodes - experimental and modelling insights, J. Power Sources 375 (2018) 300–309.
[68] W. Tang, S. Jayaraman, T.F. Jaramillo, G.D. Stucky, E.W. McFarland, Electrocatalytic activity of gold-platinum clusters for low temperature fuel cell applications, J. Phys. Chem. C 113 (2009) 5014–5024.